

The Site of Action of the Antiterminator Protein N from the Lambdoid Phage H-19B*

Received for publication, June 13, 2007, and in revised form, August 8, 2007. Published, JBC Papers in Press, August 13, 2007, DOI 10.1074/jbc.M704864200

Anoop Cheeran¹, Nanci R. Kolli, and Ranjan Sen²

From the Laboratory of Transcription Biology, Centre for DNA Fingerprinting and Diagnostics, ECIL Road, Nacharam, Hyderabad 500076, India

Transcription antitermination by N proteins of lambdoid phages involves specific interactions of the C-terminal domain of N with the elongation complex (EC). The interacting surface of N on the EC is unknown, knowledge of which is essential to understand the mechanism of antitermination. Specific cleavage patterns were generated near the active site Mg^{2+} of the RNA polymerase of an N-modified stalled EC using iron-(S)-1-(*p*-bromoacetamidobenzyl)ethylenediaminetetraacetate conjugated to the only cysteine residue in the C-terminal domain of N from a lambdoid phage H-19B. Modification of EC by N also induced conformational changes around the same region as revealed from the limited trypsin digestion and *in situ* Fe-dithiothreitol cleavage pattern of the same EC. These data, together with the previously obtained H-19B N-specific mutations in RNA polymerase, β (G1045D), and β' (P251S, P254L, G336S, and R270C) subunits, suggest that the active center cleft of the EC could be the site of action of this antiterminator. H-19B N induced altered interactions in this region of EC, prevented the backtracking of the stalled EC at the *ops* pause site and destabilized RNA hairpin- β subunit flap domain interactions at the *his* pause site. We propose that the physical proximity of the C-terminal domain of H-19B N to the active center cleft of the EC is required for the process of transcription antitermination and that it involves both stabilization of the weak RNA-DNA hybrid at a terminator and destabilization of the interactions of terminator hairpin in the RNA exit channel.

Transcription elongation complexes (EC)³ formed by the *Escherichia coli* RNA polymerase (RNAP) are exceptionally stable and highly processive (1). The stability of the EC arises from nucleic acid-protein interactions in the DNA binding site, RNA-DNA hybrid binding site, and RNA binding site (2–5). The EC dissociates from the template DNA when it encounters specific DNA sequences (intrinsic terminators) (6–8) or when

it is displaced by the nascent RNA-binding protein, Rho (9, 10). Lambdoid phages encode proteins like N and Q, and a *cis*-acting element like polymerase utilization RNA, which make the EC termination-resistant upon interaction with the elongating RNAP. This phenomenon is called transcription antitermination (11, 12).

The N protein of bacteriophage λ activates expression of the late genes by facilitating the read-through of transcription terminators present in the early genes of the phage (11, 13–15). N is a small basic protein, which binds to a specific stem-loop structure (box B of *nut* site) of the mRNA through the arginine-rich motif (ARM) present in its N-terminal domain (16, 17), and interacts with the EC through its C-terminal domain via an RNA looping mechanism (18–20). N requires several host-coded factors called Nus factors, to form a processive antitermination complex (12). The interacting surface of N on the EC is not yet known, knowledge of which is critical for understanding the mechanism of antitermination.

N-mediated antitermination of the lambdoid phage H-19B has reduced requirements for Nus factors compared with λ N. Efficient antitermination requires only NusA (21) *in vivo*, and the additional presence of NusG to achieve highly processive antitermination *in vitro* (22). This minimal requirement for host factors makes it a simpler antitermination system to reconstitute *in vitro* for biochemical studies.

Using a random mutagenesis screen, we have earlier isolated and characterized *E. coli* RNAP mutants specifically defective for H-19B N-mediated antitermination. These mutations are located very close to important structural elements of the EC, like the RNA exit channel, the lid, and the rudder (22). In this report, we have identified the regions of the EC that come physically close to the C-terminal domain of H-19B N by protein footprinting of the N-modified EC. We have also analyzed the effects of the binding of H-19B N on the interactions around the RNA-DNA hybrid at a class II pause site (23), and the interactions of the flap domain with hairpin RNA near the RNA exit channel at a class I pause site (24–27). We concluded that the C-terminal domain of H-19B N comes close to the active site Mg^{2+} and N-induced altered interactions in the active center cleft stabilize the RNA-DNA hybrid at a class I pause site and destabilize the RNA hairpin-flap domain interactions at a class II pause site. We propose that the physical proximity of the C-terminal domain of H-19B N is required for the antitermination, and the process involves both stabilization of the weak RNA-DNA hybrid at a terminator sequence and destabilization of the interactions of terminator hairpin in the RNA exit channel.

* This work was supported in part by National Institutes of Health Grant TW06185 (to R. S.) and Centre for DNA Fingerprinting and Diagnostics core funds. The costs of publication of this article were defrayed in part by the payment of page charges. This article must therefore be hereby marked "advertisement" in accordance with 18 U.S.C. Section 1734 solely to indicate this fact.

¹ A Council of Scientific and Industrial Research senior research fellow.

² To whom correspondence should be addressed: Tel.: 91-40-2715-1344 (ext. 1401); Fax: 91-40-2715-5610; E-mail: rsen@cdfd.org.in.

³ The abbreviations used are: EC, elongation complex; RB stalled elongation complex; Fe-BABE, iron-(S)-1-(*p*-bromoacetamidobenzyl)ethylenediaminetetraacetate; RNAP, RNA polymerase; ARM, arginine-rich motif; HMK, heart muscle kinase; CTD, C-terminal deletion; WT, wild type; DTT, dithiothreitol.

Site of Action of the Antiterminator N

TABLE 1
Bacterial strains and plasmids

Strains	Relevant genotype	Reference
RS38	K3093 with λ RS45 lysogen carrying pLac-nutR-3T-lacZYA fusion, <i>rpoC</i> 120 btuB::Tn10(ts), and H-19B N (pK8601) spec ^R , tet ^R	Cheeran <i>et al.</i> (22)
RS385	DH5 α transformed with pRS385; amp ^R	This study
RS422	DH5 α transformed with pRS422; amp ^R	This study
RS464	DH5 α transformed with pRS464; amp ^R	This study
RS485	MG1655 with pTRC99A- <i>E. coli</i> <i>rpoB</i> with N-terminal HMK, His tag β S531Y-NPH <i>rpoB</i> , amp ^R	From S. Borukhov
RS514	RS38 transformed with pRS513; amp ^R , spec ^R , and tet ^R	This study
RS523	DH5 α transformed with pRS523; kan ^R	This study
Plasmids		
pRS25	pTL61T with pT7A1-H-19B <i>nutR</i> (Δ cII) T1T2-LacZYA, amp ^R	Cheeran <i>et al.</i> (22)
pRS385	pRS25 with T7A1- <i>nutR-lacO-T_R'</i> fusion, amp ^R	This study
pRS422	CTD H-19BN-cloned NdeI/XhoI site of pET21b, amp ^R	This study
pRS464	N-terminal HMK-tagged H-19BN cloned into XhoI/NdeI site of pET33b(+), kan ^R	This study
pRS484	pTRC99A- <i>E. coli</i> <i>rpoB</i> with N-terminal HMK, His tag β S531Y-NPH <i>rpoB</i> , amp ^R	Laptenko <i>et al.</i> (30)
pRS513	pBAD18M- <i>E. coli</i> <i>rpoC</i> with C-terminal HMK and His tag, amp ^R	This study
pRS523	N-terminal HMK, His tag NusA cloned into XhoI/NdeI site of pET33b(+), kan ^R	This study

TABLE 2
Description of the oligonucleotides

Oligonucleotide	Description
RS2	CTTGCATGCCCTGCAGGGTCACTC, downstream oligo after T _R ' on of T7A1- <i>nutR-T_R'</i> of pRS25
RS58	ATAAACTGCCAGGAATTGGGGATC, upstream oligo of pTL61T vector sequence located upstream to the T7A1 promoter
RS63	GATTATTTGCACGGCCTCAC, upstream primer with HindIII site for <i>rpoC</i> gene in pBAD vector
RS66a	GCGGCCATATGACACGCCAGACTCAGTTC, upstream primer for H-19B N gene with NdeI site
RS70	GCTCTAGAGAATTGTGAGCGCTCACAACTCTCTAGAGC. <i>lac</i> operator palindrome flanked by XbaI site, used to clone <i>lacO</i> at the XbaI site of pRS25 plasmid
RS83	ATAAACTGCCAGGAATTGGGGATC, 5'-biotinylated RS58
RS99	GAATTGTGAGCGCTCACAAATTGGATCCGGCACCCGGGAATAGC; T7A1- <i>nutR-LacO</i> fusion amplified from pRS25 plasmid with RS83
RS137	ACGATCTGGCACCGGGCGTCTGAAGATTG; forward primer of 3134 region of <i>rpoB</i>
RS138	CAATCTTCAGCACGCCCGTGCAGATCGTC; reverse primer of 3134 region of <i>rpoB</i>
RS202	GCGCCGCTCGAGTCACTTATGTCCAAACTCATTGCGTACACAAT; downstream primer for making del-CTD (Δ 100–127 amino acids) of H-19B N
RS228	GCGCGCGAGCTTGTGGTGGTGGTGAACAGATGCACAGCTCGTTACAGAACGCCAG; downstream oligo with C-terminal HMK, 6-His tag, and SacI site complementary to C terminus of <i>rpoC</i>
RS263	CTGAAAGACTAGTCAGGATGATGGTGGCTTAGTGGTCAGATATATTGGG; downstream oligo 1 for making <i>his</i> pause template, used with RS58/RS83 on pRS25
RS264	CTGAATGCTTCCAGCACACATCGCCTGAAAGACTAGTCAGGATGATGGTTG; downstream oligo 2 for making <i>his</i> pause template, used with RS58/RS83 on the template made from RS58/RS263 pair
RS265	TTCATGCACCACTGGAAGATCTGAATGCTTCCAGCACACATCGC; downstream oligo 3 for making <i>his</i> pause template, used with RS58/RS83 on the template made from RS58/RS264 pair
RS267	GGTATGCGTGGAAACACGCACGCTACCGCTGCCCTAGTGGTCAGATATATTGGG; used for insertion of <i>ops</i> pause sequence after <i>nutR</i> site of pRS25
RS275	GGAAATTGTGAGCGCTCACAAATTCCCTCAGCACACATCGCCTGAAAGACTAG; <i>lac</i> operator sequence after 4nt of the <i>his</i> pause position, used for PCR amplification with RS83/RS265 <i>his</i> pause template
RS277	GGAAATTGTGAGCGCTCACAAATTCAACACGCACGCTACCGCTGGCC; <i>lac</i> operator sequence 4nt downstream of <i>ops</i> pause position, used for PCR amplification with RS83/RS 267 <i>ops</i> pause template

EXPERIMENTAL PROCEDURES

HMK-tagged RNA Polymerases—The heart muscle kinase (HMK) tag was introduced at the C terminus of the *rpoC* gene by PCR amplification using a primer with the HMK and His tag sequences and was cloned into pBAD18M (28) at the HindIII/SacI site. This tag did not affect cell viability and *in vivo* antitermination. C-terminal HMK-tagged RNAP was purified from this strain (RS514) following published procedures (29). The plasmid with N-terminal HMK-tagged *rpoB* was a gift from Sergei Borukhov (30). This plasmid was transformed into RS485, and the RNAP was purified as described above. Both HMK-tagged RNAPs were tested for their *in vitro* antitermination efficiencies with H-19B N. Because the RNAP preparations were not fully saturated with sigma-70, the transcription reactions were supplemented with sigma-70. Strain, plasmids, and primers used in this study are described in Tables 1 and 2.

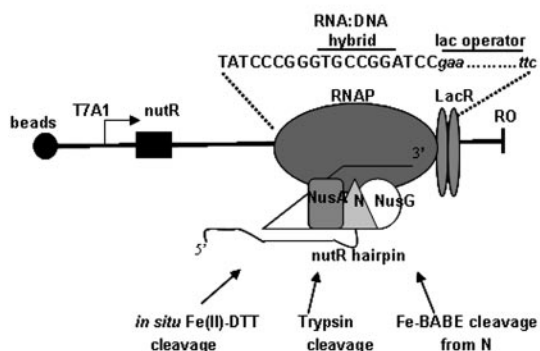
H-19B N and Nus Factors—Cloning and purification of WT H-19B N was described earlier (22). The C-terminal deletion (Δ CTD N; Δ 100–127) mutant of H-19B N was made by PCR

amplification from the WT gene and was purified following the same procedure as that for the WT protein. Cloning and purifications of NusA and NusG were also described earlier (22).

DNA Templates—A *lac* operator sequence was introduced at the downstream edge of most of the DNA templates, used for making stalled elongation complex (RB), by PCR using downstream primers with a *lac* operator sequence (see Table 2). All the templates were immobilized on the streptavidin beads via the 5'-biotin group by using biotinylated primer RS83. The *ops* pause sequence (23) was incorporated downstream to the H-19B *nutR* site by PCR amplification using primers RS83 and RS267. Plasmid pRS25 (22) was used as the template for this amplification. The *his* pause sequence was incorporated after the *nutR* site by the overlapping PCR method using the primers, RS58 (or RS83), RS263, RS264, and RS265. Transcription was initiated from the T7A1 promoter in all templates.

End Labeling of β and β' Subunits of RNA Polymerase—HMK-tagged β and β' subunits of RNA polymerase were radio-labeled with [γ -³²P]ATP (3000 Ci/mmol, Amersham Bio-

A



B

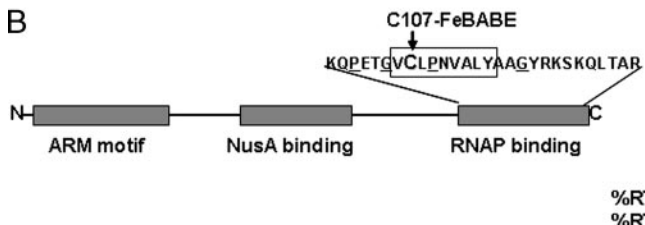
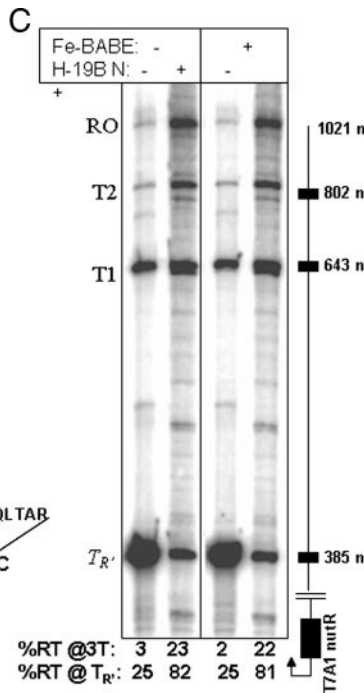


FIGURE 1. A, schematic showing the organization of the stalled EC (RB) in the presence of N, NusA, and NusG, used for the footprinting assays. The 3'-end of the RNA in this stalled EC is situated \sim 3–4 nucleotides upstream of the left edge of the lac operator sequence (32). Sequences of the RNA-DNA hybrid and the operator are indicated. B, different functional domains of H-19B N are shown. This domain organization is based on the functional domains of λ N (18) and is not drawn to the scale. The sequences of last 20 amino acids of the C-terminal region are shown. The single cysteine residue at position 107 conjugated with Fe-BABE is highlighted. Glycine and proline residues are underlined. The hydrophobic patch at the C terminus is indicated by a rectangle. C, autoradiogram showing *in vitro* antitermination in the presence of WT H-19B N, both in the Fe-BABE conjugated and unconjugated form. The template with the triple terminator cassette ($T_{R'}-T_1-T_2$) cloned downstream of the nut site is shown adjacent to the figure. The antitermination efficiencies (%RT) at the end of $T_{R'}$ and at the end of the template are calculated from the band intensities as follows: %RT@3T = $(RO)/(T_{R'} + T_1 + T_2)$ and %RT@ $T_{R'}$ = $1 - [(T_{R'})/(T_{R'} + T_1 + T_2)]$. The amount of run-off transcript is denoted as RO.

sciences) using protein kinase A (Sigma). The labeling reaction was done in buffer containing 20 mM Tris-HCl (pH 8.0), 150 mM NaCl, 10 mM MgCl₂, and 10 μ M ATP. Holoenzymes (10 μ M) were incubated with 50 units of the kinase for 1 h at 21 °C in a reaction volume of 25 μ l. Labeled RNA polymerase holoenzymes were used for Fe-BABE, Fe-DTT, and trypsin cleavage assays, without further purification.

Conjugation of H-19B N with Fe-BABE—The single cysteine (amino acid 107) at the C-terminal of H-19B N was conjugated to Fe-BABE. To remove DTT from H-19B N stock solution (20 μ M), 100 μ l of H-19B N protein was first equilibrated in exchange buffer (20 mM Tris-HCl, pH 8.0, 0.5 M NaCl, and 1 mM EDTA) and concentrated by using Amicon-10 membranes (Millipore). 0.5 mM Fe-BABE (Dojindo, Japan) was incubated with 10 μ M H-19B N in exchange buffer for 1 h at 37 °C. Unconjugated Fe-BABE was removed by passing the reaction mixture through YM 10-membranes (Millipore) and equilibrated in storage buffer (20 mM Tris-HCl (pH 8.0), 100 mM NaCl, 10% glycerol, and 1 mM EDTA). Cysteine modification was monitored by the sensitivity for 5,5'-dithiobis(2-nitrobenzoic acid).

Formation of the Stalled Elongation Complex (RB) for FE-BABE, Fe-DTT, and Trypsin Cleavages—To form the stalled elongation complex for different protein footprinting assays, we have used a DNA template containing the T7A1 promoter, and the H-19B nutR site is immobilized to the magnetic beads via a biotin group at the 5'-end of the DNA. In this template a



22-bp lac operator sequence is cloned 80 bp downstream of the nutR site (Fig. 1A). In the presence of Lac repressor, the EC (denoted as RB in different figures) is stalled at this site. 1 μ M of [γ -³²P]ATP-labeled RNAP (either RpoB- or RpoC-labeled) and 100 nM 5'-biotinylated template DNA in transcription buffer (50 mM Tris-HCl, pH 8.0, 100 mM KCl, 10 mM MgCl₂, 1 mM DTT, and 100 μ g/ml bovine serum albumin), were mixed with pre-equilibrated streptavidin magnetic beads (Promega), and the mixture was incubated for 10 min at 32 °C. Beads were washed once to remove excess RNAP and DNA, and then 100 nM Lac repressor was added. Transcription reactions were carried out in the presence of 200 μ M each of all four NTPs (Amersham Biosciences) in transcription buffer. 600 nM NusA, 400 nM NusG, 1 μ M each H-19B N, ARM H-19B N, and CTD H-19B N were also added during the reaction, when indicated. The reactions were carried out at 32 °C for 3 min and washed thrice each time with 200 μ l of transcription buffer. For Fe-DTT cleavage assays, washing was done with transcription buffer devoid of MgCl₂ to remove the Mg²⁺ from the active center. The stalled elongation complex (RB) was then used for all the cleavage assays.

Cleavage of Stalled EC by Fe-BABE-conjugated H-19B N—The RB was made in the presence of 1 μ M of Fe-BABE-conjugated WT or ARM N as described above. The cleavage reaction was initiated by adding 25 mM H₂O₂ and 100 mM ascorbic acid, and allowed to continue for different times at 32 °C. The reactions were stopped by adding 6 μ l of 5 \times SDS loading dye supplemented with 0.1 mM EDTA and were stored on ice. Samples were heated to 95 °C for 4 min prior to loading onto an 8% SDS-PAGE. Gels were exposed overnight to a phosphorimaging screen, and the bands were analyzed using phosphorimaging Typhoon 9200 and ImageQuaNT software (Amersham Biosciences).

Cleavage of Stalled EC by Fe-DTT from the Active Center—The RB complex was washed with transcription buffer without MgCl₂ and resuspended in the same buffer. Fe-DTT cleavage reactions were initiated by the addition of 5 mM DTT and 40 μ M of freshly prepared ferrous ammonium sulfate (Sigma). Reactions were terminated at different times by addition of an equal volume of 5 \times SDS-loading dye, heated to 95 °C for 4 min, and then loaded onto an 8% SDS-PAGE. The gels were analyzed by phosphorimaging.

Cleavage of Stalled EC by Trypsin—The RB complexes were incubated with 0.006 unit of trypsin for different times at 30 °C,

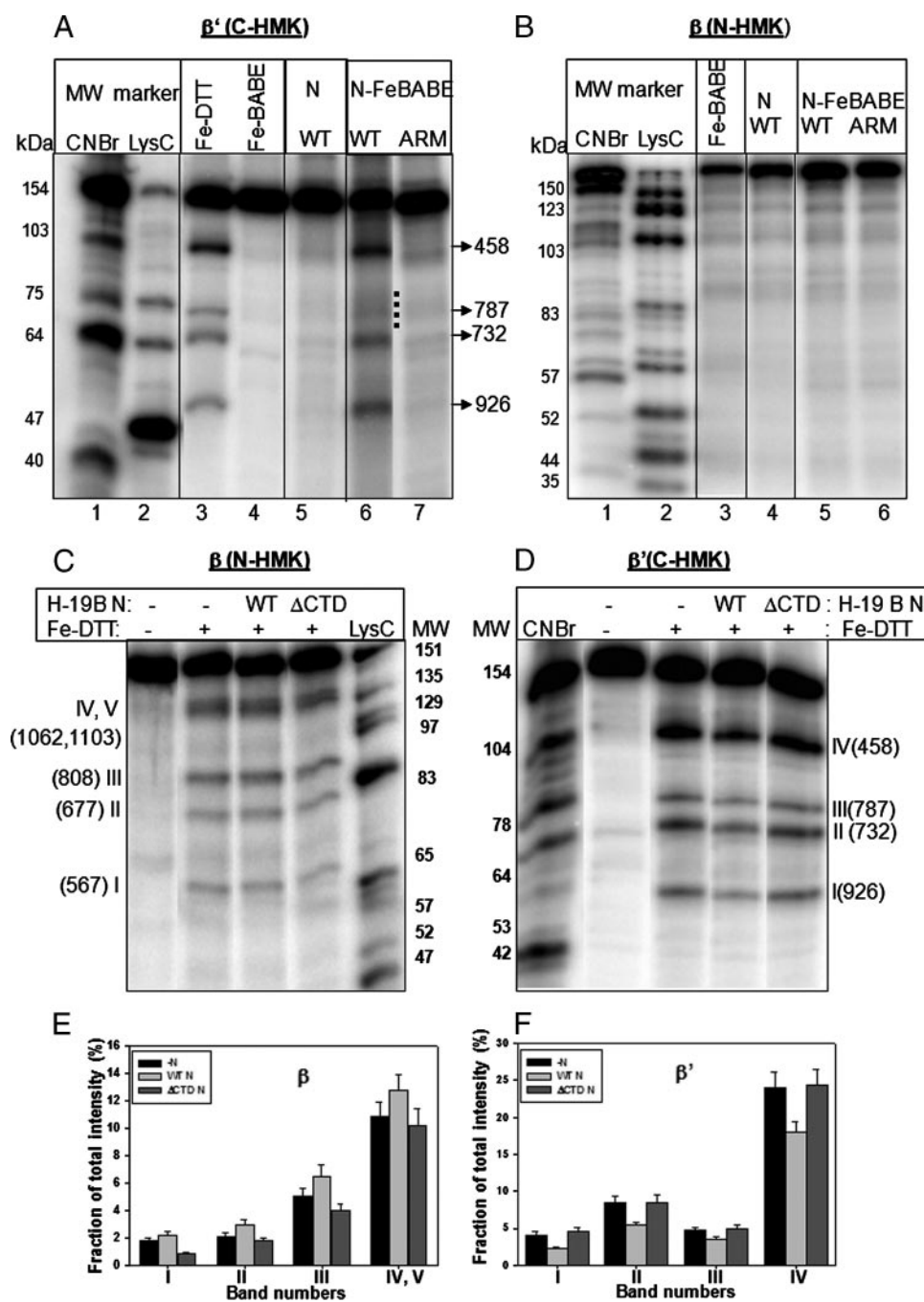


FIGURE 2. Protein cleavage profile of radiolabeled β' -subunit (A) and β -subunit (B) of RNAP in the RB generated by Fe-BABE-conjugated H-19B N. All the RB complexes in different lanes are either modified with WT or ARM mutant N. The EC is complexed with either unconjugated (A, lanes 4 and 5; B, lanes 3 and 4), or Fe-BABE conjugated WT N (lane 6 of A and lane 5 of B). In lane 7 (A) and lane 6 (B), cleavage patterns were obtained in the presence of the Fe-BABE-conjugated H-19B N having mutations in the N-terminal ARM. This mutant is unable to bind the EC. Lane 4 (A) and lane 3 (B) are the nonspecific cleavage patterns generated by free Fe-BABE when incubated with the stalled EC modified with unconjugated N. In lane 5 of A and lane 4 of B the ECs modified with unconjugated N were incubated with only H_2O_2 and ascorbic acid. The positions of the cleaved products were obtained by comparing protein markers generated by CNBr (lane 1 of both A and B) and LysC endoproteinase (lane 2 of both A and B) cleavage of the same proteins. Lane 3 of A shows the Fe-DTT cleavage pattern of the β' -subunit from the active site. Fenton reactions were performed for 1 min. The protein cleavage profiles of β -subunit (C) and β' -subunit (D) of RNAP in the stalled EC generated from the *in situ* Fe-DTT cleavage from the RNAP active site. RB complexes were made either in the absence or in the presence of WT or mutant (Δ CTD) H-19B N. Positions of the specific cleavage bands were obtained in a similar way as in A and B. Fe-DTT reactions were performed for 3 min. Normalized average intensities of each cleavage products are shown in for β -subunit (E) and β' -subunit (F). The intensities are expressed as the fraction of total intensity of all the cleavage products plus the uncleaved band. The errors in the intensity measurements are calculated from two to three independent experiments.

and the reactions were stopped by adding an equal volume of 5× SDS-loading dye. Gel electrophoresis and analysis of cleavage products were performed as described above.

Generation of Molecular Weight Markers with CNBr and LysC—Molecular weight markers of end-labeled RNA polymerase (either the β or β') were generated by CNBr (Merck)- and LysC (Sigma)-mediated cleavages following the published procedures (31). Calibration curves were generated from the migration of these cleavage products, and the locations of the cleavage products in Figs. 2 and 3 were identified from the polynomial fit of the calibration curves.

Transcription Assays on *ops* and *his* Pause Templates—For pause assays, the templates with T7A1-nutR-*ops* and T7A1-nutR-*his* constructs were used. First, a 23-mer elongation complex (EC_{23}) was made by initiating the transcription with 175 μ M adenylyl-(3'-5')-uridine, 5 μ M each of GTP and ATP, 2.5 μ M CTP, and [α - 32 P]CTP (3000 Ci/mmol, Amersham Biosciences) on both the templates. To determine the kinetics of elongation on the *ops* pause template, the EC_{23} was chased in the presence of 100 μ M each of UTP, CTP, and ATP and 10 μ M GTP. When required, NusA, NusG, WT, and Δ CTD N were added to the chase solution. Aliquots (5 μ l) were removed at the indicated times and mixed with an equal volume of formamide loading dye. For assays on the *his* pause template, EC_{23} was chased in the presence of 150 μ M of UTP, CTP, and ATP and 10 μ M of GTP. Concentrations of different components used in these were as follows: 20 nM RNAP, 5 nM DNA template, 100 nM LacI, 200 nM H-19B N, 300 nM NusA, and 200 nM NusG. Products were analyzed on 8% sequencing gels.

To generate RB at *ops* and *his* pause sites, 5'-biotinylated templates with *ops* or *his* pause sequences fused to *lac* operator sequences were used. The stalled ECs (RB) using Lac repressor as a roadblock were formed essentially

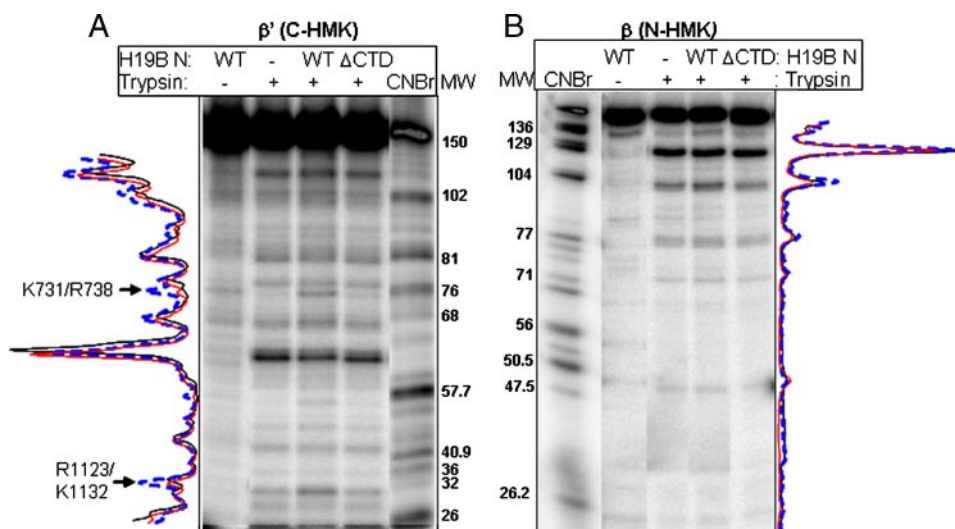


FIGURE 3. Limited trypsin digestion pattern of β' (A) and β (B) subunits of RNAP in the RB complex in the absence and presence of either WT or mutant (Δ CTD) H-19B N. The band intensities of each cleavage products are shown adjacent to each autoradiogram. The colors are coded as follows: blue, in the presence of WT N; black, in the absence of N; red, in the presence of mutant N. In the case of the β' subunit, two cleavage products that are enhanced in the presence of WT N are indicated. The nearest two arginine and lysine residues corresponding to these bands are indicated. The positions of the cleavage products were identified from the molecular weight markers generated by CNBr treatment. Trypsin digestions were performed for 1 min.

as described for the protein cleavage assays. Nus factors and N were added to this chase reaction when required. RB complexes were washed with transcription buffer to remove the NTPs. The indicated amount of GreB (Fig. 6) or sodium pyrophosphate (Fig. 7) was then added to the respective RB complexes. Products were analyzed on 8% sequencing gels.

Fe-DTT Cleavage of RNA at the ops Pause—RB complexes were formed at the *ops* pause, essentially the same way as described above. The RB was washed with transcription buffer without $MgCl_2$ and resuspended in the same buffer. Fe-DTT cleavage reactions were initiated by the addition of 5 mM DTT and 40 μ M of freshly prepared ferrous ammonium sulfate (Sigma). Reactions were terminated by addition of phenol, and the products were analyzed on 6% sequencing gels.

RESULTS

Design of N-modified Stalled EC for Biochemical Probing—We have designed a stalled EC (RB) modified with NusA, NusG, and H-19B N (both WT and mutant), using Lac repressor as a roadblock (schematic shown in Fig. 1A). The *lac* operator sequence is placed about 80 bp downstream of the *nutR* site to facilitate the *nutR*-hairpin dependent binding of H-19B N to the RB. This stalled EC remains active over the time period of *in vitro* assays (22, 32). In all the protein footprinting assays, this RB was formed using radiolabeled RNAP. The radiolabeling was achieved through the HMK tag sequences at the N terminus of β and the C terminus of β' subunits of RNAP, for the detection of cleavage products generated from the Fe-BABE-, Fe-DTT-, and Trypsin-mediated cleavage reactions.

WT H-19B N has a single cysteine residue (amino acid 107) at its C-terminal RNAP binding domain (Fig. 1B). This single cysteine residue was conjugated with the hydroxyl radical generating reagent Fe-BABE (33). Hydroxyl radicals generated *in situ* will cleave the peptide backbones of the different domains

of RNAP situated within 12 \AA of the C-terminal cysteine residue of the H-19B N bound to the EC, and thereby will define the regions of EC close to the C-terminal of N. To ascertain that the interaction surface defined by this method is physiologically relevant, we assayed the antitermination efficiency of the Fe-BABE-labeled N at the end of a triple terminator cassette (22). We observed that this Fe-BABE-labeled N has a similar antitermination efficiency as unlabeled N (Fig. 1C). Other single cysteine derivatives in the C-terminal domain that we made yielded inactive N (data not shown), so we restricted our assays only to those with this Fe-BABE-conjugated N.

Fe-BABE-labeled N Generated Cleavage Patterns of β and β' Subunits of RNA Polymerase in the Stalled EC

The N protein conjugated to Fe-BABE at Cys-107 generated specific cleavage products only in the β' subunit (lane 6, Fig. 2A) but not in the β subunit of RNAP of the stalled EC (Fig. 2B, compare lanes 5 with 3, 4, and 6). The cleavage was not observed when Fe-BABE was conjugated to a mutant N defective for binding to EC (ARM N; lane 7 of Fig. 2A). Also stalled EC modified with un-conjugated N did not produce any cleavage pattern over the background (lane 5 of Fig. 2A), and incubation of free Fe-BABE with the EC modified with un-conjugated N (lane 4 of Fig. 2A) also did not produce any specific cleavage product. This suggests that this cleavage pattern in lane 6 of Fig. 2A originated from the Fe-BABE conjugated to WT N and only when this conjugated N is specifically bound to the EC. The Fe-BABE-mediated cleavage sites on β' were mapped close to amino acid residues 458 (conserved region D), 732 (conserved region F), and 926 (conserved region G). Cleavages at these three sites are usually obtained (compare lanes 3 and 6 of Fig. 2A) when hydroxyl radical is generated from the active site by replacing Mg^{2+} with Fe^{2+} (30, 34) (also see below). A major difference observed was that no cleavage by Fe-BABE was detected near amino acid 787 (compare lanes 3 and 6 of Fig. 2A; indicated as dashed lines in the gel) of β' subunit. In the same experimental set-up, Fe-BABE-labeled N did not cleave the RNA or DNA in the RNA-DNA hybrid (data not shown).

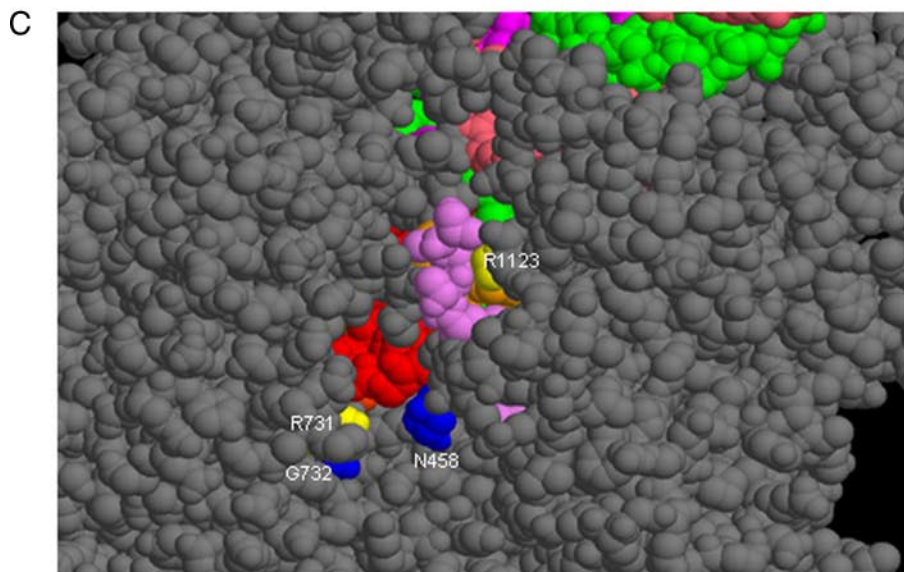
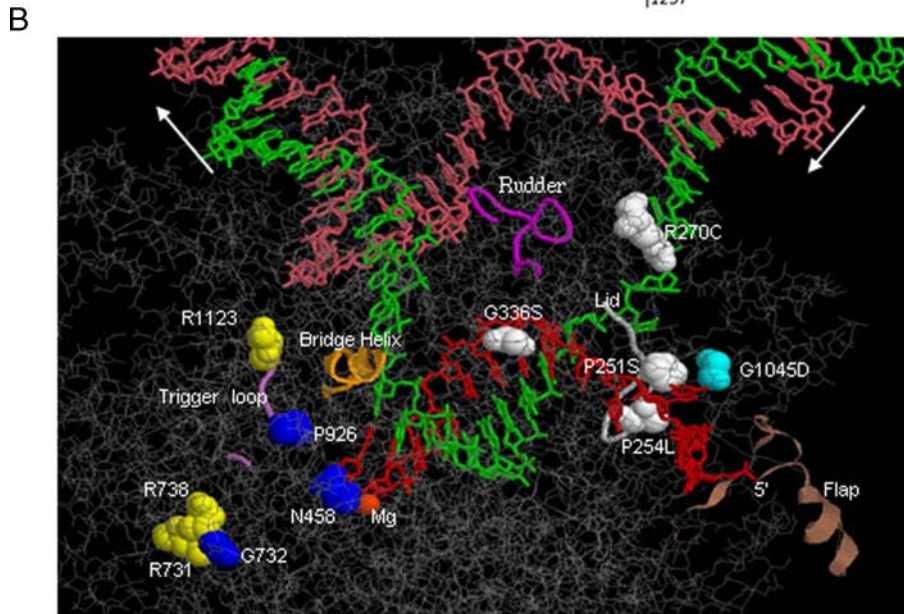
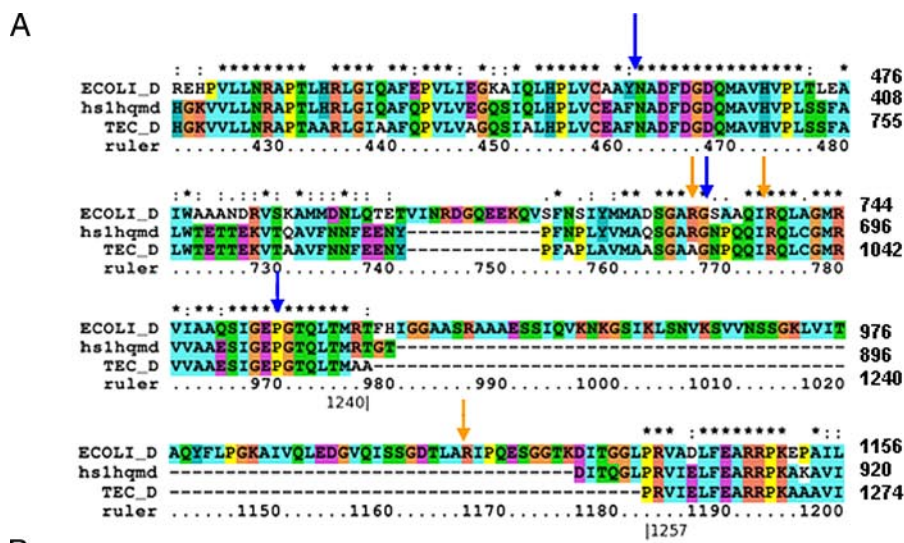
It can be argued that the similarity of cleavage pattern may have arisen from the natural affinity of the Fe^{2+} moiety of Fe-BABE for the metal center at the active site. We ruled out this possibility because of the following reasons. If the Fe^{2+} moiety of the Fe-BABE occupies the Mg^{2+} binding site, it should have generated cleavage patterns in β subunit, in the DNA, and in the RNA as has been observed earlier for Fe-DTT cleavage from the active site of the EC (34). Moreover the reactions were performed in the presence of excess Mg^{2+} , and the occupation of a Fe^{2+} in the active site requires the removal of Mg^{2+} (34; also see

Site of Action of the Antiterminator N

lane 4 of Fig. 2A). So it is unlikely that Fe^{2+} of the Fe-BABE moiety has replaced the active site Mg^{2+} . However, if due to one or more unknown reasons, having this Fe^{2+} ion of the N-conjugated Fe-BABE moiety transferred to the active site would still require the C-terminal of N to be in the vicinity of the active site. Alternatively, it is possible that, due to this natural affinity of Fe-BABE toward the metal center, the C-terminal domain of N is drawn toward the vicinity of the active center. But this did not affect the antitermination property of H-19B N (Fig. 1C). Therefore, we suggest that the observed cleavage patterns arose simply from the physical proximity of the C-terminal domain of N to this region of β' subunit. It should also be mentioned that NusA and NusG present in the stalled EC were not cleaved by Fe-BABE attached at this cysteine position (data not shown).

Localized $\text{Fe}(\text{II})$ -mediated Cleavage Pattern of the N-modified EC—Physical proximity of the C-terminal domain of H-19B N to the active center may induce some conformational changes in this region. To probe such changes, if any, we compared the localized hydroxyl radical cleavage from the active site and the trypsin cleavage patterns of the N-modified and unmodified stalled ECs.

The localized hydroxyl radical generated by replacing the active site Mg^{2+} of free RNAP with Fe^{2+} in the presence of DTT yields characteristic cleavage patterns in the β and β' subunits (30, 34). The major cleavages in β subunit are at Pro-567, Asn-677, Asn-808, Pro-1062, and Val-1103 and those in β' are at Asn-458, Gly-732, Ala-787, and Pro-926 positions. Any conformational change in and around the active center may change this cleavage pattern. We observed similar cleavage patterns in the stalled EC as those reported earlier (30, 34) for free RNAP (Fig. 2, C and D). In the presence of WT H-19B N, there were modest changes in the intensity of the bands. In general, the



intensity of the bands in the β' subunit was reduced when the EC was modified specifically with WT N (Fig. 2, E and F). This may indicate N-induced subtle structural rearrangements around the active center. Changes in cleavage pattern in the β subunit were not significant.

Trypsin Cleavage Pattern of N-modified EC—Conformational changes in the EC was then probed by limited trypsin cleavage of the β and β' subunits. The trypsin digestion patterns in the presence of WT N did not reveal protection of any regions of the β and β' subunits (Fig. 3, A and B). However, binding of N induced enhanced cleavage at β' positions Arg-1123/Lys-1132 and Lys-731/Arg-738, but not in β . The resolution of the gel was not high enough to identify the exact amino acids corresponding to the enhanced cleavage products. The enhancement in intensity was induced specifically by WT N, because it was not detected in the presence of Δ -CTD N, a mutant N that does not bind to the EC. These two cleavage positions of enhanced intensities are close to the active site (Fig. 4, B and C), which also suggest that N induces conformational changes around the active center. It should also be noted that these two sites are exposed to the surface of the EC (Fig. 4C).

Mapping of the Cleavage Positions in the Model Structure of EC—We have earlier described RNAP mutations (P251S, P254L, R270C, and G333S in β' and G1045D in β subunit) specific to H-19B N action, which are located in and around the RNA exit channel, the lid, and rudder elements of the EC (22). To find the spatial relationship of the N-induced cleavage sites with the positions of those mutations, we localized both the cleavage sites and the positions of the mutations on the available model of EC, developed on the basis of the crystal structures of *Thermus aquaticus* RNA polymerase (35), the yeast RNA polymerase II EC (36), and the cross-linking data on protein-nucleic acids interactions in the EC of *E. coli* RNAP (4). We first determined the equivalent amino acids of these mutations and the cleavage sites in the model structure by structural alignment (Fig. 4A) using ClustalX (37). Fig. 4B shows the location of the cleavage sites together with H-19B N-specific mutations obtained earlier. Interestingly, the cleavage sites obtained from Fe-BABE or Trypsin are located close to the active site and did not overlap with the sites of the mutations. The space-filled version of the model (Fig. 4C) shows that both the Trypsin cleavage sites and two of the Fe-BABE-induced cleavage sites are visible through the secondary channel and located close to the surface.

The Fe-BABE-induced cleavage sites are found to be \sim 30–60 Å away from the positions of the different mutations. Therefore, it is unlikely that the C-terminal domain of H-19B N is placed close to the region defined by the mutations, because the hydroxyl radicals will not be able to travel over this long

distance to generate cleavages near active site Mg^{2+} . One possible explanation for this observation is that the C-terminal domain comes physically close to the active site Mg^{2+} and that this N-induced interaction near the active site exerts allosteric effects in the regions defined by the location of the mutations. Mutations close to the active site would be lethal, so they were not obtained from our previous genetic screen (22).

N Prevents Reversible Backtracking at ops Pause Sequences—The antiterminators N and Q can suppress pausing during elongation (38–40). Results from protein footprinting experiments (Fig. 2), and from earlier mutational analyses (22) suggest that H-19B N may modulate interactions around the RNA-DNA hybrid as well as in the RNA exit channel. Therefore, we assayed the effect of H-19B N on two well defined pause sequences, namely *ops* and *his* pauses, which involve altered interactions in these two regions. At the *ops* pause sequence, pausing occurs due to the backtracking of the EC, which is dependent on the sequence of the RNA-DNA hybrid (23). Pausing at *his* pause sequence is proposed to be mediated by interaction of a RNA-hairpin with the flap domain of β -subunit located near the RNA exit channel (23–27). The sequence at the *his* pause codes for RNA that folds into a hairpin near the exit channel.

We followed the pause kinetics through the *ops* pause sequence cloned downstream of the *nutR* site, both in the absence and presence of either WT or mutant H-19B N proteins (Fig. 5A). The amount of paused complex was plotted against time (Fig. 5B). In the presence of WT N, pausing efficiency (denoted as “ a ” in the equation of exponential decay; shown in the inset of Fig. 5B) was not affected, whereas the rate of escape (denoted as “ λ ” in the equation) from the paused state was three times faster than that observed in the absence of WT N. This result suggests that N does not prevent the EC from entering the paused state but reduces the half-life of this conformational state possibly by disfavoring the backtracking of EC, which is an important component of this type of pausing (23). To determine whether N prevents backtracking at this sequence, the EC was stalled at this site by using Lac repressor as a roadblock (Fig. 5C). Backtracking of the stalled EC was monitored by GreB-induced cleavage of the RNA (41, 42) and by the Fe-DTT-mediated cleavage of the 3'-end of the RNA from the active site of the EC (43). In the absence of WT N, the EC was sensitive to GreB-induced cleavage (Fig. 5D), and Fe-DTT-mediated cleavage of the RNA was also observed at an internal position (marked as “cleaved RNA” in Fig. 5E). These are the indications of the backtracking of the EC at this pause site. In the presence of WT N, sensitivity of EC for GreB was significantly reduced (Fig. 5D), and Fe-DTT-mediated cleavage was also not observed (Fig. 5E). These two results suggest that

FIGURE 4. Location of cleavage sites and the H-19B N specific mutations on the model of EC. A, structural alignment of the relevant regions of β and β' subunits of *E. coli* RNAP with the equivalent regions of *T. aquaticus* RNAP using ClustalX. Positions of the cleavage sites are indicated by arrows. Color codes are in accordance with the ClustalX notations. hs1ddqc and hs1hqm are the Homstrad database identity numbers of *T. aquaticus* RNAP C (*rpoB*) and D chains (*rpoC*), respectively. *TEC_C* and *TEC_D* stand for ternary elongation complex C and D chains, respectively. Blue arrows are for Fe-BABE-mediated and yellow arrows are for trypsin-mediated cleavage sites. B, an expanded view of the nucleic acid framework in the of the model structure of EC using RASMOL. Locations of different mutations (in white and cyan) and cleavage sites (in blue for Fe-BABE and in yellow for trypsin cleavage sites) are shown in space-filled representation in the wire-framed gray background of other parts of RNAP. The colors of template DNA, non-template DNA, and RNA are green, pink, and red, respectively. Active site Mg^{2+} is shown in orange. Flexible loop structures of “rudder,” “lid,” bridge helix, trigger loop, and flap domains are also indicated. White arrows indicate the direction of transcription. C, space-filled model of the EC surrounding the secondary channel area showing the surface accessibility of the cleavage sites. Colors are the same as those in B.

Site of Action of the Antiterminator N

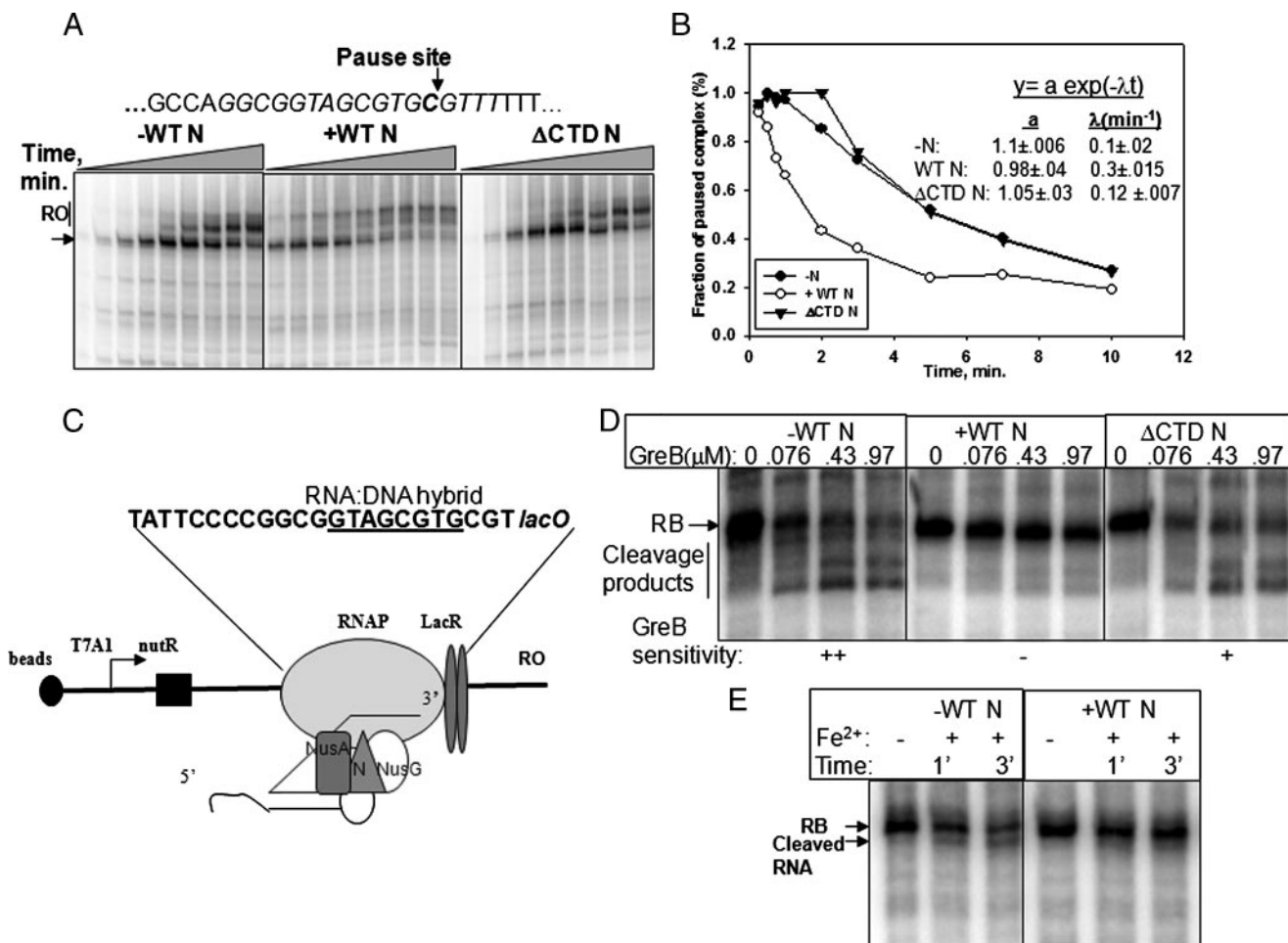


FIGURE 5. Anti-pausing activity at the *ops* pause sequence. *A*, autoradiogram showing the time course of transcription elongation through the *ops* pause sequence (indicated by arrow) both in the absence and presence of either WT or ΔCTD H-19B N. The pause sequence and pausing site are shown above the autoradiogram. Run-off product is indicated as "RO." *B*, amount of fraction of paused complex obtained under different conditions is plotted against time. The plots were fitted to the equation of exponential decay using SIGMAPLOT to calculate the rate (λ) of escape from the paused state and efficiency (a) of pausing. The equation and average values obtained from these calculations are shown in the inset. *C*, schematic showing the N-modified EC stalled at *ops* pause site using Lac repressor as a roadblock. At this position the RNA-DNA hybrid contains the *ops* pause sequence. This stalled EC is used to probe backtracking at this sequence by GreB sensitivity and by Fe-DTT-mediated cleavage of RNA in the RNA-DNA hybrid from the active site of the EC. *D*, autoradiogram showing the GreB-induced cleavage of the RNA in the RB at the *ops* pause site. Different concentrations of GreB were added to the RB complexes either unmodified or modified with WT or ΔCTD H-19B N, and incubated for 3 min. Cleavage products are indicated. The sensitivity toward GreB is indicated by "++" (highly sensitive), "+" (moderately sensitive), and "−" (not sensitive). Concentrations of GreB are indicated. *E*, cleavage of the 3'-end of RNA in the RNA-DNA hybrid by Fe²⁺. A cleaved product is visible in the absence of N and is indicated as "cleaved RNA." The time of the reaction is indicated.

H-19 B N prevents backtracking at *ops* pause site. This observation is specific to WT N, because its mutant derivative did not elicit this response.

N Destabilizes the Flap Domain-RNA Hairpin Interactions at His Pause Sequences—Next, we followed the pause kinetics through the *his* pause site cloned downstream of the *nutR* sequence (Fig. 6*A*). The amount of paused complex was plotted as described above (Fig. 6*B*). As in the case of the *ops* pause, the pausing efficiency at the *his* pause did not change significantly in the presence of WT N, whereas the rate of escape from the paused state increased by ~5-fold (see the inset of Fig. 6*B* for the rate constant values). The effect of N on the *his* pause was more pronounced than at the *ops* pause. The dwelling time in this paused state depends on the stability of the flap domain-RNA hairpin interaction (27). As binding of N only affected the pause half-life, it is possible that it did not affect the formation of the pause hairpin but, rather, weakened the flap-hairpin interaction. It has also been shown that the flap-hairpin inter-

action at this pause site leads to catalytic inactivation of the EC (27). Therefore, if the presence of H-19B N destabilizes this interaction, it will also prevent the catalytic inactivation caused by the RNA hairpin. To test this hypothesis, the EC was stalled by Lac repressor at the pause site, NTPs were removed by washing, and the catalytic competence of the stalled EC was tested by the pyrophosphorylation reaction (Fig. 6*C*). Fig. 6*D* shows that the 3'-end of the RNA of this stalled EC exactly matched the pause site (compare the lanes 3 and 4, lanes 10 and 11, lanes 17 and 18). Accumulation of RNA cleavage products (marked as "P_i cleavage") induced by pyrophosphate was significantly faster in the presence of WT H-19B N. This effect was specific to WT N, because the pyrophosphorylation reaction was slow and inefficient both in the absence of N or in the presence of ΔCTD N. We suggest that the flap domain-RNA interaction is destabilized or significantly weakened in the N-modified EC and thereby preventing the catalytic inactivation. Alternatively, the presence of H-19 B N might have prevented the formation

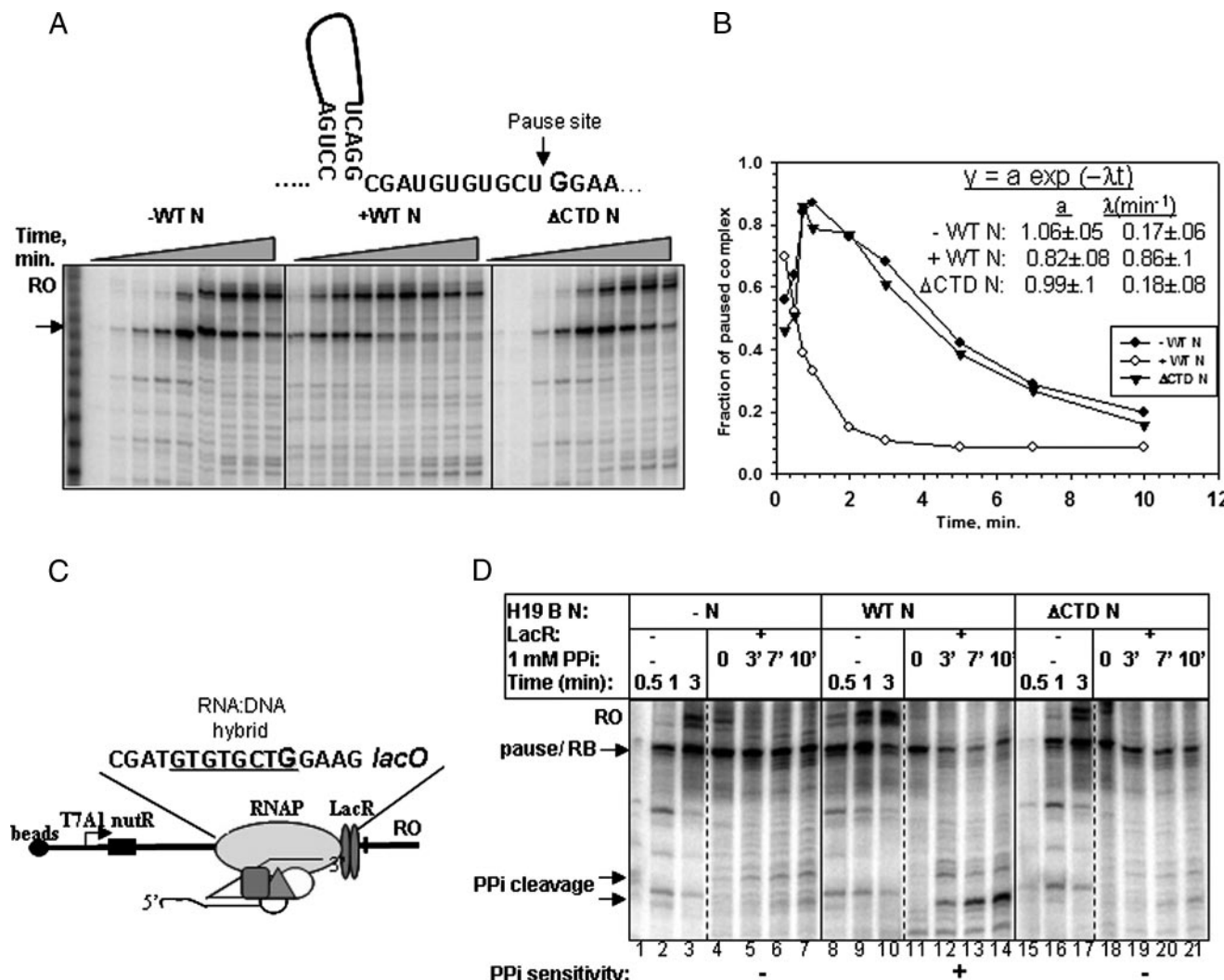


FIGURE 6. Anti-pausing activity at the *his* pause sequence. *A*, autoradiogram showing the time course of transcription elongation through the *his* pause sequence (indicated by arrow) both in the absence and presence of either WT or ΔCTD H-19B N. Pause sequence, pausing site, and pause-hairpin are shown above the autoradiogram. Run-off product is indicated as "RO." *B*, amount of fraction of paused complex obtained under different conditions is plotted against time. The analyses of the plots were done in the same way as in Fig. 5, and the average values of the kinetic parameters obtained from these calculations are shown in the inset. *C*, schematic showing the N-modified EC stalled at the *his* pause site using Lac repressor as a roadblock. At this position the RNA-DNA hybrid contains the *his* pause sequence, and the 3'-end matches the pausing position (marked by an arrow). This set-up was used to probe the catalytic competence of the N-modified and unmodified ECs at the *his* pause. *D*, autoradiogram showing the RNA cleavage from pyrophosphorolysis reactions in the presence of sodium pyrophosphate from N-modified and unmodified stalled ECs at the *his* pause site. Time courses of elongation through this pause site (lanes 1–3, 8–10, and 15–17) are shown along with each stalled complex to compare the pausing and stalling positions. Pyrophosphorolysis reactions were performed by adding 1 mM sodium pyrophosphate (PPI) to each of the stalled complexes, and incubated for indicated times. The cleavage products are indicated. Sensitivity toward PPI is marked as either "+" (sensitive) or "-" (not sensitive).

of "hyper-translocated" state of the 3'-end of the RNA, which has been postulated as the characteristic of the ECs at the *his* pause site (23).

DISCUSSION

Specific interactions of the bacteriophage-derived transcription antiterminators with RNAP during transcription elongation are mandatory to achieve antitermination. Although several mutations in RNAP defective for N-dependent antitermination have been reported earlier (22, 44–50), the interaction surface of this antiterminator on the EC remains elusive. Knowledge of this is essential to understand the mechanism of antitermination. In this report, we present evidence for the region of EC that comes physically

close to the C-terminal domain (the RNAP binding domain) of N from lambdoid phage H-19B. The cleavage pattern derived from Fe-BABE-conjugated N bound to a stalled EC revealed that the C-terminal of N approaches close to the active site Mg^{2+} (Figs. 2 and 4). This interaction induced specific conformational changes nearby to this region (Figs. 3 and 4). From these data, together with the previously obtained H-19B N-specific mutations in RNAP, β (G1045D), and β' (P251S, P254L, G336S, and R270C) subunits, we propose that the active center cleft of the EC broadly defines the site of action of this antiterminator (Fig. 4*B*). We also showed that this interaction of the C-terminal domain of N with the EC blocked the backtracking of the EC at a class II pause site (Fig. 5) and prevented the catalytic inactivation caused by

Site of Action of the Antiterminator N

the RNA hairpin-flap domain interaction in the RNA exit channel at a class I pause site (Fig. 6).

The transcription antitermination at an intrinsic terminator can be achieved by stabilizing the weak U-rich RNA-DNA hybrid, by preventing or delaying the folding of RNA hairpin as well as its interaction in the RNA exit channel. Based on the protein footprinting data and the analysis of N-modified ECs stalled at class I and class II pause sites, we propose that physical proximity of the C-terminal domain of N near the active site Mg^{2+} stabilizes the 3'-end of the weak RNA-DNA hybrid directly by altering the interactions around it, which in turn, allosterically destabilizes the RNA hairpin interactions in the distal RNA exit channel. The proposal that N affects the RNA hairpin interactions in the exit channel is consistent with earlier proposals of improper or delayed folding of the RNA-hairpin in the exit channel of N-modified EC (22, 38).

It is evident from the space-filling model (Fig. 4C) that Fe-BABE cleavage sites are not on the surface of the EC. So the C-terminal domain of H-19B N has to be inserted into the EC to generate this cleavage pattern (Fig. 2A). The presence of a hydrophobic patch (Fig. 1B) in the C-terminal encompassing the cysteine residue might help this region to be inserted into the core of the EC. N protein from bacteriophage λ is disordered in solution, and its C-terminal domain remains unfolded even after the N-terminal domain binds to the nut RNA (18, 51). It is possible that lack of proper secondary structure helps this region to be inserted into the core of the EC.

How does the C-terminal of H-19B N access the interior of the EC? This region of EC can be accessed either through the secondary channel (used by Gre factors and NTPs (52)) or through the RNA exit channel. To make the antitermination process kinetically efficient, the C-terminal of N should be inserted into the EC when the *nut* site is close to the EC. Also as the central part of N interacts to NusA (53), it can act as an anchor for the C-terminal N-EC interactions. Therefore it is possible that the location of NusA on the EC in the N-NusA-EC complex will determine the insertion site of the C-terminal domain of N in the EC. There can be several possibilities. The C-terminal domain may insert through the secondary channel and interact with the regions of EC close to the active site Mg^{2+} and exert an allosteric effect on the regions close to the RNA exit channel. Alternatively, the presence of the N-NusA complex at the floor of the RNA exit channel, assuming that NusA in the NusA-N complex binds to the N-terminal coiled-coil domain of β' -subunit (52), can widen the exit channel so that the regions close to the 3'-half of the RNA-DNA hybrid become more accessible to the free C-terminal end of N. The other possibility is, like the related transcription factor Nun from lambdoid phage HKO22 (54), the C terminus of the H-19B N can also access the active site through the downstream DNA-binding cleft of the EC.

Do our results define a generalized interaction surface for all the N proteins? Sequence alignment of the C-terminal amino acids from different N proteins revealed that this region is highly conserved among the majority of the known N proteins (Fig. 7A). Therefore, it is possible that the nature of interaction of these N proteins with the EC will also be similar. However, the C-terminal domains of more well characterized N proteins

	A	
Lambda	68 -ESNLQRIERKQNQRTWY--SKP-GERGITCSGRQKIKGKSIPLI	107
phi-21	60 --KKAEEVERKQNRIYY--SKPRSEMGVTCVGRQKIKLGSKPLI	99
H19-B	88 -RAAIIVYANEFGHKQPE-TGVCLPNVALYAAGYRKSKQLTAR--	127
933W	88 -RAAIIVYANEFGHKQPE-TGVCLPNVAIYAAGYRKSKQLTAR--	127
HK97	88 -RAAIIVYANEFGHKQPE-TGVCLPNVALYAAGYRKSKQLTAR--	127
Ni12	75 MRAEVITL-TTLTRKYE-GSTCLPNVALYAAGYRKSKQLTAR--	114
VT2 Sa	75 MRAEVITL-TTLTRKYE-GSTCLPNVALYAAGYRKSKQLTAR--	114
HK620	51 -AASLGSIRKKAEECS-GSICLPNVAIYAAGYRKSKQLTAR--	90
P22	61 --TKAISLAGTQKEVEGGSVLLPGVALYAAGHRKSKQITAR--	100
PhageL	39 --SIFGCDVPDASHEVAKAIRDVTKAISLAGTQKQKVEVQR--	78
HKO22Nun	73 --KALATPFPRDVEKIE--DEKYEDVMHRVVNHAAHQNPNNKKWS	112

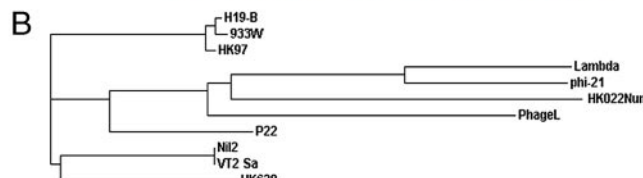


FIGURE 7. A, ClustalW alignment of the C-terminal domain of N proteins from different phages. H-19B N and its related N proteins are marked with a box. Amino acid residues are indicated. B, phylogram of different N proteins.

from λ and its closer relatives, ϕ -21 and phage L, are very much different, and they belong to a distinct phylogenetic group (Fig. 7B). It will be interesting to know whether the C terminus of λ N also interacts with the same region of EC and follows the same mechanism of antitermination.

Acknowledgments—We thank Drs. Lucia Rothman-Denes, T. Ramasarma, Jeffrey W. Roberts, Rupinder Kaur, Irina Artsimovitch, and other laboratory members for critically reading the manuscript. We also thank M. Sridhar Achary for help in calculating the distances between different elements from the structural model of EC.

REFERENCES

1. Arndt, K. M., and Chamberlin, M. J. (1990) *J. Mol. Biol.* **213**, 79–108
2. Nudler, E., Avetissova, E., Markovtsov, V., and Goldfarb, A. (1996) *Science* **273**, 211–217
3. Sidorenkov, I., Komissarova, N., and Kashlev, M. (1998) *Mol. Cell* **2**, 55–64
4. Korzheva, N., Mustaev, A., Kozlov, M., Malhotra, A., Nikiforov, V., Goldfarb, A., and Darst, S. A. (2000) *Science* **289**, 619–625
5. Darst, S. A. (2001) *Curr. Opin. Struct. Biol.* **11**, 155–162
6. Nudler, E., and Gottesman, M. E. (2002) *Genes Cells* **7**, 755–768
7. Uptain, S. M., and Chamberlin, M. J. (1997) *Proc. Natl. Acad. Sci. U. S. A.* **94**, 13548–13553
8. von Hippel, P. H. (1998) *Science* **281**, 660–665
9. Richardson, J. P. (2002) *Biochim. Biophys. Acta* **1577**, 251–260
10. Banerjee, S., Chalissery, J., Bandey, I., and Sen, R. (2006) *J. Microbiol.* **44**, 11–22
11. Friedman, D. I., and Court, D. L. (1995) *Mol. Microbiol.* **18**, 191–200
12. Weisberg, R. A., and Gottesman, M. E. (1999) *J. Bacteriol.* **181**, 359–367
13. Das, A., Pal, M., Mena, J. G., Whalen, W., Wolska, K., Crossley, R., Rees, W., von Hippel, P. H., Costantino, N., Court, D., Mazzulla, M., Altieri, A. S., Byrd, R. A., Chattopadhyay, S., DeVito, J., and Ghosh, B. (1996) *Methods Enzymol.* **274**, 374–402
14. Greenblatt, J., Nodwell, J. R., and Mason, S. W. (1993) *Nature* **364**, 401–406
15. Van Gilst, M. R., and von Hippel, P. H. (2000) *Methods Enzymol.* **323**, 1–31
16. Chattopadhyay, S., Garcia-Mena, J., DeVito, J., Wolska, K., and Das, A. (1995) *Proc. Natl. Acad. Sci. U. S. A.* **92**, 4061–4065
17. Lazinski, D., Grzadzierska, E., and Das, A. (1989) *Cell* **59**, 207–218
18. Mogridge, J., Legault, P., Li, J., Van Oene, M. D., Kay, L. E., and Greenblatt, J. (1998) *Mol. Cell* **1**, 265–275
19. Nodwell, J. R., and Greenblatt, J. (1991) *Genes Dev.* **5**, 2141–2151

20. Whalen, W. A., and Das, A. (1990) *New Biol.* **2**, 975–991
21. Neely, M. N., and Friedman, D. I. (2000) *Mol. Microbiol.* **38**, 1074–1085
22. Cheeran, A., Babu Suganthan, R., Swapna, G., Bandey, I., Achary, M. S., Nagarajaram, H. A., and Sen, R. (2005) *J. Mol. Biol.* **352**, 28–43
23. Artsimovitch, I., and Landick, R. (2000) *Proc. Natl. Acad. Sci. U. S. A.* **97**, 7090–7095
24. Chan, C. L., Wang, D., and Landick, R. (1997) *J. Mol. Biol.* **268**, 54–68
25. Artsimovitch, I., and Landick, R. (1998) *Genes Dev.* **12**, 3110–3122
26. Toulokhanov, I., Artsimovitch, I., and Landick, R. (2001) *Science* **292**, 730–733
27. Toulokhanov, I., and Landick, R. (2003) *Mol. Cell* **12**, 1125–1136
28. Sen, R., King, R. A., Mzhavia, N., Madsen, P. L., and Weisberg, R. A. (2002) *Mol. Microbiol.* **46**, 215–222
29. Kashlev, M., Nudler, E., Severinov, K., Borukhov, S., Komissarova, N., and Goldfarb, A. (1996) *Methods Enzymol.* **274**, 326–334
30. Laptenko, O., Lee, J., Lomakin, I., and Borukhov, S. (2003) *EMBO J.* **22**, 6322–6334
31. Nechaev, S., Yuzenkov, Y., Niedziela-Majka, A., Heyduk, T., and Severinov, K. (2002) *J. Mol. Biol.* **320**, 11–22
32. King, R. A., Sen, R., and Weisberg, R. A. (2003) *Methods Enzymol.* **371**, 207–218
33. Meares, C. F., Datwyler, S. A., Schmidt, B. D., Owens, J., and Ishihama, A. (2003) *Methods Enzymol.* **371**, 82–106
34. Mustaev, A., Kozlov, M., Markovtsov, V., Zaychikov, E., Denissova, L., and Goldfarb, A. (1997) *Proc. Natl. Acad. Sci. U. S. A.* **94**, 6641–6645
35. Zhang, G., Campbell, E. A., Minakhin, L., Richter, C., Severinov, K., and Darst, S. A. (1999) *Cell* **98**, 811–824
36. Gnatt, A. L., Cramer, P., Fu, J., Bushnell, D. A., and Kornberg, R. D. (2001) *Science* **292**, 1876–1882
37. Thompson, J. D., Gibson, T. J., Plewniak, F., Jeanmougin, F., and Higgins, D. G. (1997) *Nucleic Acids Res.* **25**, 4876–4882
38. Gusarov, I., and Nudler, E. (2001) *Cell* **107**, 437–449
39. Rees, W. A., Weitzel, S. E., Das, A., and von Hippel, P. H. (1997) *J. Mol. Biol.* **273**, 797–813
40. Roberts, J. W., Yarnell, W., Bartlett, E., Guo, J., Marr, M., Ko, D. C., Sun, H., and Roberts, C. W. (1998) *Cold Spring Harbor Symp. Quant. Biol.* **63**, 319–325
41. Borukhov, S., Sagitov, V., and Goldfarb, A. (1993) *Cell* **72**, 459–466
42. Komissarova, N., and Kashlev, M. (1997) *Proc. Natl. Acad. Sci. U. S. A.* **94**, 1755–1760
43. Nudler, E., Mustaev, A., Lukhtanov, E., and Goldfarb, A. (1997) *Cell* **89**, 33–41
44. Georgopoulos, C. P. (1971) *Proc. Natl. Acad. Sci. U. S. A.* **68**, 2977–2981
45. Ghysen, A., and Pironio, M. (1972) *J. Mol. Biol.* **65**, 259–272
46. Sternberg, N. (1976) *Virology* **73**, 139–154
47. Jin, D. J., Cashel, M., Friedman, D. I., Nakamura, Y., Walter, W. A., and Gross, C. A. (1988) *J. Mol. Biol.* **204**, 247–261
48. Schauer, A. T., Cheng, S. W., Zheng, C., St Pierre, L., Alessi, D., Hidayetoglu, D. L., Costantino, N., Court, D. L., and Friedman, D. I. (1996) *Mol. Microbiol.* **21**, 839–851
49. Obuchowski, M., Wegrzyn, A., Szalewska-Palasz, A., Thomas, M. S., and Wegrzyn, G. (1997) *Mol. Microbiol.* **23**, 211–222
50. Szalewska-Palasz, A., Strzelczyk, B., Herman-Antosiewicz, A., Wegrzyn, G., and Thomas, M. S. (2003) *Arch. Microbiol.* **180**, 161–168
51. Van Gilst, M. R., and von Hippel, P. H. (1997) *J. Mol. Biol.* **274**, 160–173
52. Borukhov, S., Lee, J., and Laptenko, O. (2005) *Mol. Microbiol.* **55**, 1315–1324
53. Bonin, I., Muhlberger, R., Bourenkov, G. P., Huber, R., Bacher, A., Richter, G., and Wahl, M. C. (2004) *Proc. Natl. Acad. Sci. U. S. A.* **101**, 13762–13767
54. Watnick, R. S., and Gottesman, M. E. (1999) *Science* **286**, 2337–2339

The Site of Action of the Antiterminator Protein N from the Lambdoid Phage H-19B

Anoop Cheeran, Nanci R. Kolli and Ranjan Sen

J. Biol. Chem. 2007, 282:30997-31007.
doi: 10.1074/jbc.M704864200 originally published online August 13, 2007

Access the most updated version of this article at doi: [10.1074/jbc.M704864200](https://doi.org/10.1074/jbc.M704864200)

Alerts:

- [When this article is cited](#)
- [When a correction for this article is posted](#)

[Click here](#) to choose from all of JBC's e-mail alerts

This article cites 54 references, 17 of which can be accessed free at
<http://www.jbc.org/content/282/42/30997.full.html#ref-list-1>